Applied Catalysis B: Environmental 339 (2023) 123127

Contents lists available at ScienceDirect

Applied Catalysis B: Environmental

journal homepage: www.elsevier.com/locate/apcatb

Superior performance in passive NO_x adsorption over an Al-rich Beta zeolite supported palladium

Jian Li [a], Kai Fan [a], Yulong Shan [b], Sen Wang [c], Juan Zhang [d], Weibin Fan [c], Hong He [b], Xiyu Zhao [e], Xiangju Meng [a,*], Feng-Shou Xiao [a,d,**]

[a] Key Lab of Applied Chemistry of Zhejiang Province, Department of Chemistry, Zhejiang University, Hangzhou 310058, PR China
[b] Research Center for Eco-Environmental Sciences, Chinese Academy of Sciences, Shuangqing Road 18, Beijing 100085, PR China
[c] State Key Laboratory of Coal Conversion, Institute of Coal Chemistry, Chinese Academy of Sciences, Taiyuan 030001, PR China
[d] Key Lab of Biomass Chemical Engineering of Ministry of Education, College of Chemical and Biological Engineering, Zhejiang University, Hangzhou 310058, PR China
[e] Beijing Normal University-Hong Kong Baptist University United International College, Zhuhai 519000, PR China

ARTICLE INFO

Keywords:
Beta zeolite
Al-rich
Palladium
Passive NO_x adsorbers (PNA)
Al pairs

ABSTRACT

Passive NO_x adsorption (PNA) has been regarded as a new technology for NO_x elimination at low temperatures in heavy diesel vehicles (HDV) during the cold-start period. For this process, it has been reported that zeolite-supported Pd samples are good adsorbents for the PNA, where the large pores and low Si/Al ratios (SAR) in the zeolites are favorable for the PNA. Therefore, we chose Al-rich Beta with both abundant Al species and large 12-membered ring pores as a support to load Pd species for preparation of the PNA adsorbents. As a result, 1 % Pd/Beta-4 showed much higher NO adsorption capacity than 1 % Pd/Beta-13, which is assigned to more Al pairs in the Beta-4 than those in the Beta-13. Even after hydrothermal treatment at 750 °C for 16 h, the 1 % Pd/Beta-4 still exhibited high passive NO capacity. These features should be helpful for the control of NO_x emissions in the future.

1. Introduction

NO_x has been regarded as one of the major sources of air pollution, which are mainly resulted from the combustion of fossil fuels [1,2]. Notably, heavy diesel vehicles (HDV) produce more than 70 % NO_x with less than 10 % automobiles. Thus, increasingly stringent emission legislations have been enacted since the end of the last century [3]. To solve this problem, selective catalytic reduction of NO_x with NH_3 (NH_3-SCR) in oxygen-rich exhausts has proven to be a highly efficient technology for the control of NO_x emissions [4–6], where Cu-SSZ-13 has been identified as one of the best SCR catalysts for HDVs after a long-term evaluation of the catalytic performance, stability, and durability [7]. However, critical issue emerged at low temperatures, *e.g.* many NO_x are emitted during the cold-start period before the light-off temperature (> 200 °C) for SCR catalysts. Therefore, efficient technologies for elimination of NO_x at low temperature are strongly desirable.

Trapping NO_x during the cold-start stage and releasing them after SCR system working has been regarded as a good candidate for solving the NO_x emission at low temperatures [8–16]. For the NO_x trapping, passive NO_x adsorption (PNA) has drawn much attention [17,18]. Typically, metal oxides (*e.g.* CeO_2, Al_2O_3 *etc.*) supported Pd or Pt have been extensively investigated [17,19–22]. Recently, zeolites supported Pd species are very interesting as PNA materials due to their higher trapping efficiency, better storage capacity, and longer resistance to sulfur poisoning [23–29]. Szanyi et al. have systemically studied the performance of Pd supported on MFI, CHA, and *BEA zeolites with the same Pd loadings under the same conditions, showing that Pd/*BEA exhibited the best performance at low adsorption temperature, indicating the key role of zeolite topology for PNA performance [30]. In addition, Si/Al ratios (SAR) of the zeolites on the PNA performance are also investigated [31,32], showing that Al-rich zeolites prefer the dispersion of ionic Pd^{2+}, which could be attributed to the fact that more negative charges in the Al-rich zeolites have more sites interacting with Pd^{2+}, *i.e.* high Pd^{2+} ion-exchange ability. Therefore, it is deduced that zeolites with large pores (cages) and low SAR should be good candidates for the PNA. However, the hydrothermal stability of conventional zeolites with large pores and low SAR (*e.g.* X and Y zeolites) is questionable for NO_x emission-control system in HDVs.

* Corresponding author.
** Corresponding author at: Key Lab of Applied Chemistry of Zhejiang Province, Department of Chemistry, Zhejiang University, Hangzhou 310058, PR China.
E-mail addresses: mengxj@zju.edu.cn (X. Meng), fsxiao@zju.edu.cn (F.-S. Xiao).

https://doi.org/10.1016/j.apcatb.2023.123127
Received 5 June 2023; Received in revised form 19 July 2023; Accepted 21 July 2023
Available online 28 July 2023

Typically, the SAR of Beta zeolite, another zeolite with relatively large porous architecture, is always fixed in a very small range of 10–15, which is generally prepared in the presence of tetraethylammonium hydroxide (TEAOH) as an organic template [33–36]. In 2008, organotemplate-free synthesis of Beta zeolite have been reported and later investigations confirm that the hydrothermal stability of such Beta is very high, even the SAR could be reduced as low as 4.0 [37]. Such Al-rich Beta zeolite exhibited superior catalytic performances in many reactions [38–47]. Particularly, Al-rich Cu(Fe)-Beta exhibited enhanced catalytic properties and high hydrothermal stability in NH_3-SCR reaction [45]. Moreover, the Al-rich Beta zeolite supported Pt catalyst is very active, which is assigned to the combined contribution of highly dispersed Pt nanoparticles and a high density of acidic sites in the zeolite framework [44]. Considering the advantages of the Al-rich Beta with large pores, low SAR, and excellent hydrothermal stability, it is chosen the Al-rich Beta (Beta-4, SAR at 4.0) zeolite support Pd as an adsorbent for investigation of the PNA property in this work. The results showed that the Pd/Beta-4 exhibited much higher NO adsorption capacity than conventional Beta (Beta-13, SAR at 13.0) supported the same Pd loading.

2. Experimental

2.1. Materials

Sodium hydroxide (NaOH ≥ 96.0 %), sodium aluminate ($NaAlO_2$, Al_2O_3 ≥ 41.0 %), ammonium chloride (NH_4Cl ≥ 99.5 %), sodium chloride (NaCl ≥ 99.5 %) and hydrogen fluoride (HF in aqueous, 40 %) were purchased from Sinopharm Chemical Reagent Co., Ltd. Tetraethylammonium hydroxide (TEAOH, 25 %) was supplied by BASF. Fumed silica (SiO_2) was purchased from Shenyang Chemical Industry Co., Ltd. Palladium (II) nitrate dihydrate ($Pd(NO_3)_2{\cdot}2H_2O$, 99 %, Pd 39.5 %) was purchased from Beijing InnoChem Science & Technology Co., Ltd. Cobalt nitrate hexahydrate ($Co(NO_3)_2{\bullet}6H_2O$, 99.99 %) was purchased from Shanghai Macklin Biochemical Co., Ltd.

2.2. Catalyst preparation

Al-rich Beta (Beta-4) and conventional Beta (Beta-13) was prepared according to the literature [34,37]. The details were described in the supplementary data.

Pd/Beta-4 was prepared by ion-exchange of $Pd(NO_3)_2$ solution. As a typical run, the desired amount of $Pd(NO_3)_2$ was dissolved into deionized water to get $Pd(NO_3)_2$ solution with a certain concentration. Then, 1 g of H-Beta zeolite was added into 100 mL of $Pd(NO_3)_2$ solution. After filtration, dryness at 100 °C under air, and calcination in air at 650 °C for 4 h, the sample was finally obtained, which was designated as *x*%Pd/Beta-4, where "*x*" represents Pd loading. Similarly, Pd/Beta-13 samples were prepared.

Hydrothermal treatment was performed at 750 °C for 16 h in a flow reactor with GHSV = 40,000 L/g·hr in a gas mixture containing 10 % H_2O in air. The treated 1 % Pd/Beta-4 % and 1 %Pd/Beta-13 were denoted as 1 %Pd/Beta-4–750HTA and 1 %Pd/Beta-13–750HTA, respectively.

2.3. Characterization

All of samples were characterized by X-ray diffraction (XRD), N_2 adsorption-desorption isotherms, inductively coupled plasma (ICP), X-ray photoelectron spectra (XPS), UV-Vis-NIR reflectance spectra, ^{29}Si NMR and ^{27}Al NMR spectra. The details were described in the supplementary data.

Na^+ titration was carried to quantify the percentage of exchangeable Pd^{2+}. As a typical run, 50 mg sample of different Pd loading was stirred in 1 M NaCl solution (50 mL) at 80 °C for 1 h, then the solid was separated by centrifugation. After second ion-exchange of Na^+ with Pd^{2+}, the Na^+ concentration in the solution was measured. The amount of Pd species remained in zeolites was quantified by ICP-OES.

For quantifying the concentration of the Al sites in the framework, the Co-Beta-4 and Co-Beta-13 were prepared by ion-exchanging method. As a typical run, 1 g H-form zeolite was mixed with 50 mL 0.5 M NaCl solution at room temperature for 3 h and repeated for 3 times. To obtain Co-form samples, 1 g Na-exchanged powder was mixed with 150 mL 0.05 M $Co(NO_3)_2$ solution at room temperature for 8 h. After the repeated treatment three times, Co-form samples were obtained.

3. Results and discussion

3.1. Standard NO storage tests

NO storage properties of the Pd/Beta-4 and Pd/Beta-13 have been evaluated in a gaseous mixture that simulates the cold start exhaust emissions from typical diesel vehicles. Fig. 1 shows profiles of NO adsorption at 110 °C for the Pd/Beta-4 and Pd/Beta-13. Notably, rapid decrease in the concentration of NO was observed for the two samples as soon as they were exposed to the NO containing feed gas. Both reach nearly 95 % NO trapping efficiency (*i.e.* NO concentrations below 10 ppm) at the same time, and the duration for maintaining the NO trapping efficiency above 95 % is varied from 54 to 126 s. Thereafter, NO storage approaches saturation and returns to the inlet level. As observed in Fig. 1, the duration time for conventional Beta zeolite is similar to that of the previous work [47], but the duration time for the Al-rich Beta zeolite is nearly longer than 2 times of the conventional Beta zeolite, indicating the high NO adsorption capacity of the Pd/Beta-4, compared with the Pd/Beta-13. Furthermore, NSA (NO storage amount) and NPR (mol $_{NO}$/mol $_{Pd}$ Ratio) were used to evaluate the NO adsorption capacity of the adsorbents. 1 %Pd/Beta-13 gives the NSA and NPR at 50 μmol $_{NO}$/g $_{catalyst}$ and 0.54, respectively, which are also similar to those of the previous work [30,47]. In contrast, the 1 %Pd/Beta-4 exhibits the NSA and NPR at 85 μmol $_{NO}$/g $_{catalyst}$ and 0.92, respectively, which are much higher than those of the 1 %Pd/Beta-13.

In order to investigate whether the adsorbent can meet the requirements of low-temperature adsorption and high-temperature desorption of NO_x. Fig. 2 shows NO and NO_2 release profiles of the Pd/Beta-4 and Pd/Beta-13 after adsorption of NO at 110 °C, and both present two desorption peaks. Notably, NO desorption started at about 130 °C. With increasing temperature, the 1 %Pd/Beta-13 showed nearly 100 % NO release until the temperature reached to 320 °C, while a full desorption of NO on the 1 %Pd/Beta-4 was about 420 °C, which might be related to that the 1 %Pd/Beta-4 has higher NO adsorption capacity than the 1 %Pd/Beta-13. This result confirms that 1 %Pd/Beta-4 can function as PNA absorbent and be beneficial for the elimination of NO_x in the subsequent SCR systems. At the same time, it is also observed the signals associated NO_2, which might be resulted from two reasons. One is due to the oxidation by Pd oxide or the oxygen atoms on the framework during the adsorption, and the other is formed by oxidation of NO

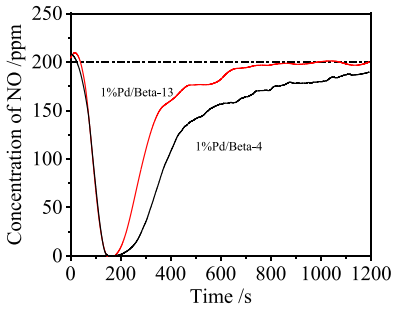

Fig. 1. NO uptake profile of 1 % Pd/Beta at 110 °C. Conditions: 150 mg of the sample, 200 ppm of NO, 200 ppmCO, 10 % O_2, and 5 % H_2O balanced with N_2 at a flow rate of 200 sccm.

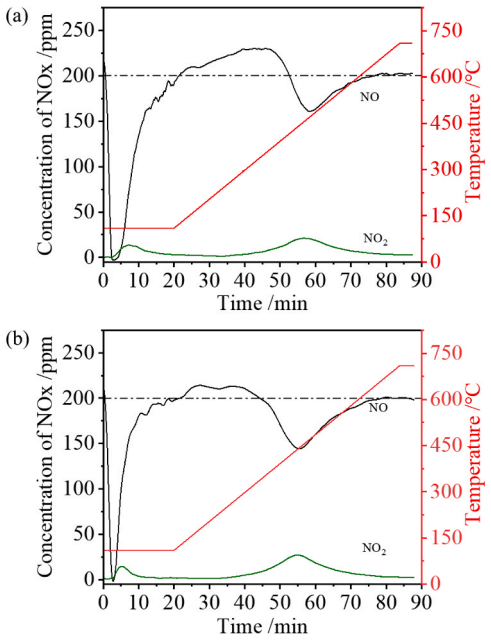

Fig. 2. NO_x uptake/release profile of the (a) 1 % Pd/Beta-4 and (b) 1 % Pd/Beta-13. NO_x adsorption at 110 °C for 10 min, followed by TPD (10 °C/min linear ramp rate). Conditions: 150 mg of the sample, 200 ppm of NO, 200 ppm CO, 10 % O_2, and 5 % H_2O balanced with N_2 at a flow rate of 200 sccm.

with O_2 above 400 ℃.

3.2. Pd species

To reveal the superior performance in the PNA over the Pd/Beta-4, the state of Pd species was investigated by XPS, Na^+ titration, and operando IR techniques.

In order to investigate the oxidation state of Pd species, XPS analysis and H_2-TPR were used to distinguish different Pd species. Fig. 3 shows XPS analysis of the 1 %Pd/Beta-4 % and 1 %Pd/Beta-13, giving bands at 337 eV ($3d_{5/2}$) and 342.4 eV ($3d_{3/2}$) for Pd^{2+} species and bands at 338.9 eV ($3d_{5/2}$) and 344.3 eV ($3d_{3/2}$) for Pd^{4+} species [48,49]. After deconvolution, it is clear that the 1 %Pd/Beta-4 has more Pd^{2+} species (88 % in total Pd species) than the 1 %Pd/Beta-13 (73 % in total Pd species). Furthermore, the TPR signal in Fig. S4 at ~220 ℃ and ~450 ℃ of both absorbents are attributed to Pd^{2+} located in the channel of *BEA zeolite [50].

Na^+ titration was used to quantify the Pd^{2+} species. Table 1 presents the amount of exchangeable (*i.e.*, isolated) Pd^{2+} cations using a NaCl solution titration, since only isolated Pd^{2+} cations can be exchanged by Na^+ into the aqueous phase [51]. For the Pd/Beta-4, with increasing Pd loading from 0.44 % to 1.47 %, Pd/Al ratios of the samples increase linearly and the percentage of Pd^{2+} in total Pd species basically remain at 95–97 %. However, for the Pd/Beta-13, with the increase of Pd loading, Pd/Al ratios shows a nonlinear increase, and the percentages of exchangeable Pd^{2+} cations greatly varied from 96 % to 56 %. This phenomenon means that the SAR of zeolites is important for adjusting the state of Pd species and the zeolites with low SAR favor the generation of Pd^{2+} cations (Fig. S2 and Fig. S3), in good agreement with the results from XPS data.

NO and CO are regularly used as probe molecules to study adsorption states of metal species. Fig. 4 shows FTIR spectra of NO or CO adsorbed on the 1 %Pd/Beta-4. NO adsorption on the 1 %Pd/Beta-4 has bands at 2188, 1872, and 1828 cm^{-1} (Fig. 4b). The band at 2170 cm^{-1} is attributed to the $\nu_{N\text{-}O}$ vibration of NO^+ species located in the extra-framework positions of the zeolite [51,52], while the bands at 1872 and 1828 cm^{-1} are assigned to Pd^{2+}(NO) complex and Pd^+(NO), respectively [53]. NO^+

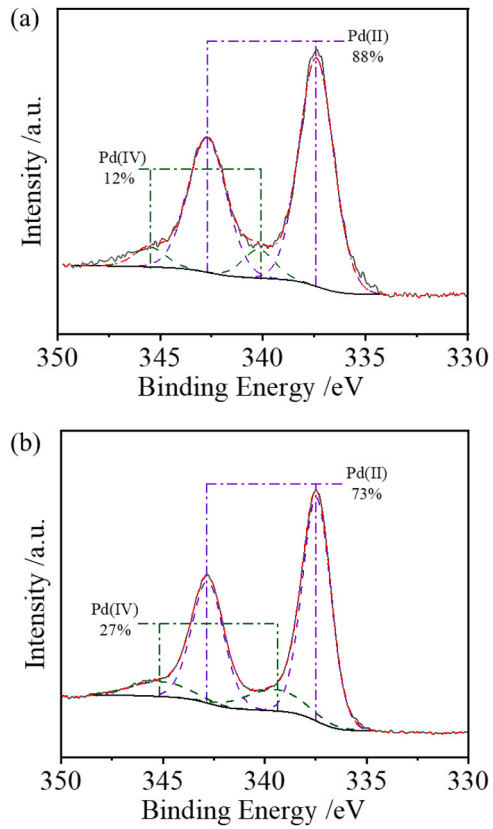

Fig. 3. Pd *3d* XPS spectra of the (a) 1 % Pd/Beta-4 and (b) 1 % Pd/Beta-13.

Table 1
Si/Al and Pd/Al ratios, total Pd, and Na^+-exchangeable Pd^{2+} in the Pd/Beta samples.

Series	Si/Al	Loading of Pd (wt%)	Pd/Al	Isolated Pd^{2+}/ Pd
1	4	0.44	0.018	95.2 %
2	4	0.77	0.035	97.4 %
3	4	0.98	0.048	94.2 %
4	4	1.36	0.061	94.7 %
5	4	1.47	0.066	95.5 %
6	13	0.36	0.035	96.0 %
7	13	0.71	0.076	82.8 %
8	13	0.83	0.087	82.4 %
9	13	1.02	0.115	78.1 %
10	13	1.17	0.124	55.9 %

is formed by a direct electron transfer from the NO radical to Pd^{2+} [54]. This electron transfer reduces Pd^{2+} to Pd^+, releasing the vacant cationic site onto the nitrosyl ion to form NO^+ [52–58]. CO adsorption on the 1 % Pd/Beta-4 (Fig. 5b) exhibits two kind of the bands associated with Pd^+(CO) (2113 cm^{-1}) [59] and Pd^{2+}(CO) (2155, 2132, 2096 and 2076 cm^{-1}) [59,60], where Pd^+ is formed by the reduction of ion-exchanged Pd species with CO [61]. Notably, the Pd^0(CO) species (below 2000 cm^{-1}) are almost undetectable [59,62], supporting that isolated Pd cations are dominant in the 1 %Pd/Beta-4, which are well consistent with those from XPS and ion-exchange techniques.

When the sample exposed to the gaseous mixture of NO + CO + O_2, a new peak at 1800 cm^{-1} was observed in FTIR spectra (Fig. S6), which can be assigned to Pd^{2+}(CO)(NO) species. It has been reported that CO can improve NO adsorption behavior because CO could act as a reductant to lower the Pd oxidation state, where the partially reduced Pd could bond strongly to NO_x species by strengthening the covalent bond through π-backdonation. Besides, the selective formation of carbonyl-nitrosyl Pd complex [Pd^{2+}(NO)(CO)] can also enhance the resistance to water

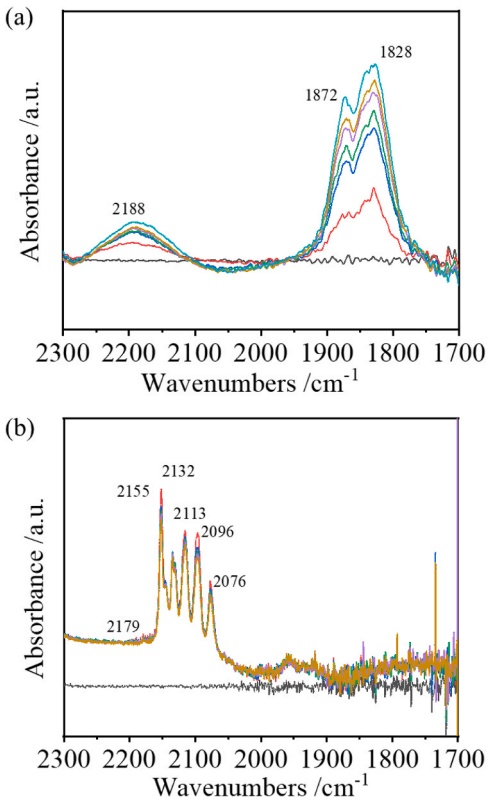

Fig. 4. FTIR spectra recorded during (a) 200 ppm NO adsorption and (b) 200 ppm CO adsorption on the 1 % Pd/Beta-4.

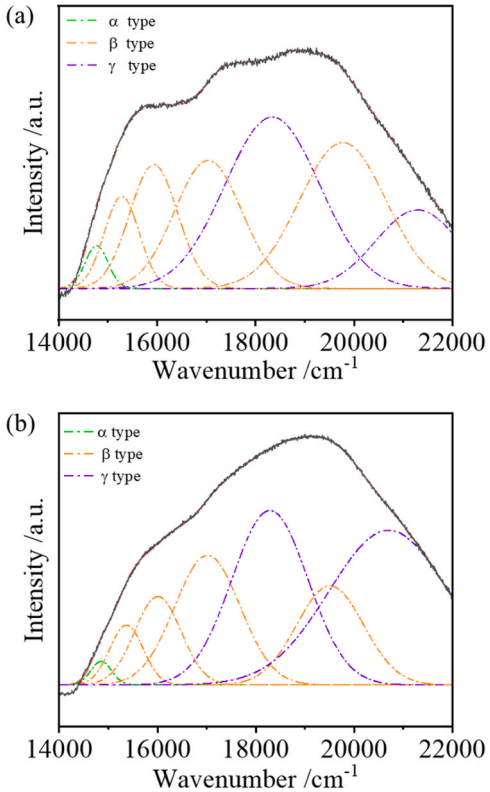

Fig. 5. Normalized UV-Vis-NIR spectra of the (a) Co-Beta-4 and (b) Co-Beta-13 evacuated at 500 °C for 3 h and spectra simulations.

poisoning [61,63].

3.3. Al pairs

Fig. S7 showed ^{29}Si NMR and ^{27}Al NMR deconvolution profiles of the 1 %Pd/Beta-4 % and 1 %Pd/Beta-13. In Fig. S7a, all of them showed similar peaks. The peaks at −115 ppm, −111 ppm, −107 ppm were assigned to Si(4Si) species [64–66]. The peak at −103 ppm was assigned to Si(3Si, Al) or Si(3Si, 1OH)species [64–66]. The peak at −99 ppm was assigned to Si(2Si, 2Al) [64–66]. The results of ^{27}Al NMR measurements were displayed in Fig. S7b , showing resonances at 0 ppm and 53 ppm, assigning to the octahedral extra-framework Al and tetrahedral Al in the framework, respectively [67,68]. The presence of extra-framework Al might mean the existence of PdO clusters [69].

The content of Al pairs of zeolites strongly influences ion-exchange capacity of divalent-cations. If the two Al atoms are located at different rings of building units, it only balance protons or monovalent cation complexes rather than the ion-exchange of Pd^{2+} [70]. Therefore, the formation of Al pairs in the zeolite framework is very important for the ion-exchange of Pd^{2+}.

To investigate the distributions of Al sites in Beta-4 and Beta-13 zeolites, ion-exchange of Co(II) as probing cations was monitored by DR UV–vis spectroscopy (Fig. 5) and ICP tests. Table 2 presents the ICP analysis from Co-Beta-4 and Co-Beta-13 samples that the proportion of Al_{pair} ($\approx Al_{close}$) and $Al_{isolated}$ ($Al_{unpair} + Al_{single}$) values are about 63.2 % and 36.8 % for Beta-4, as well as 43.8 % and 56.2 % for Beta-13, respectively. Obviously, more Al pairs of Beta-4 can accommodate more Pd^{2+} ions than Beta-13 to improve NO storage capacity.

Furthermore, DR UV-Vis spectra of dehydrated Co(II)-BEA/zeolites exhibited a broad complex absorption ranging from 14,000 to 22,000 cm^{-1} ascribed to the *d-d* transitions of high-spin bare Co(II) ions coordinated exclusively with oxygen atoms of framework rings [71,72]. The bare Co(II) ions should be exclusively balanced in that zeolite by AlO_4^- of Al pairs in the α, β, and γ cationic sites [72,73]. Seven Gaussian curves (Fig. 5) were employed in the decomposition Co(II) spectra, and the assignment of each curves were according to the publication by Mlekodaj et al. [72] The proportion of the three types of cationic sites were listed in Table 2. Evidently, the β sites in the deformed 6MRs of Beta-4 (62.9 %) are much more than Beta-13 (52.1 %), which were identical with the discovery reported by Dedecek et al., who pointed out that β sites are more helpful to stabilize the Pd ions [72]. Furthermore, H_2-TPR curves of the samples (Fig. S4) exhibited two peaks at 220 ℃ and 450 ℃ assigned to the occupy of Pd ions in the γ and β sites, reported previously [50]. Notably, the percentage of Pd ions in β sites calculated from the TPR curve are 63 % and 53 % for 1 %Pd/Beta-4 % and 1 % Pd/Beta-13, which was very similar to those in DR UV-Vis spectra of these samples. These results indicate that higher proportion of Al_{pair} of Beta-4 would be accommodate more Pd^{2+} in the deformed 6MR, which is very helpful for improving NO storage capacity.

3.4. NO storage capacity of hydrothermal aged 1 % Pd/Beta-4

Hydrothermal aging at high temperatures is a typical deactivation pathway in emission control catalysts [74–76]. After aging at 750 °C, the loading of Pd and the SAR (Si/Al) remained ~1 wt% and ~4 according to the ICP-OES. XRD patterns of the samples showed that *BEA structure was remained without obvious decreased crystallinity. NO adsorption experiments of the hydrothermal aged 1 % Pd/Beta-4

Table 2
Distributions of different types of Al atoms in Co^{2+}-exchanged Beta-4 and Beta-13 as measured by DR UV–vis spectroscopy and ICP tests.

Samples	Al_{pair} (%)	Al_{unpair} (%)	α type (%)	β type (%)	γ type (%)
Beta-4	63.2	36.8	0.9	62.9	35.3
Beta-13	43.8	56.2	1.8	52.1	47.0

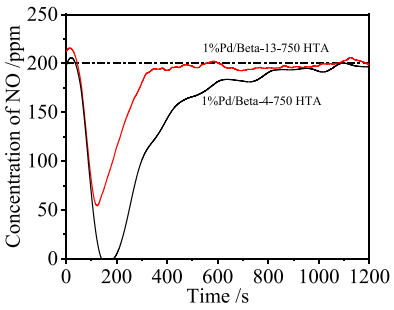

Fig. 6. NO uptake profiles of the 1 % Pd/Beta-4–750 HTA and 1 % Pd/ Beta-13–750 HTA at 110 °C. Conditions: 150 mg of the sample, 200 ppm of NO, 200 ppm CO, 10 % O_2, and 5 % H_2O balanced with N_2 at a flow rate of 200 sccm.

showed that the duration still maintain the NO trapping efficiency above 90 % (66 s, Fig. 6), which is still longer than that of the fresh 1 % Pd/Beta-13. Calculated NPR and NSA of 1 % Pd/Beta-4–750 HTA is 0.58 and 54 μmol $_{NO}/g_{catalyst}$, which are better than those of fresh 1 % Pd/Beta-13, indicating the high hydrothermal stability of the 1 % Pd/Beta-4. In contrast, the NO adsorption capacity of the 1 % Pd/Beta-13–750 HTA with NPR and NSA were estimated to be 0.23 and 22 μmol $_{NO}/g_{catalyst}$, indicating more than 57 % loss of the adsorption capacity for the fresh 1 % Pd/Beta-13.

4. Conclusion

In summary, we have designed efficient Pd species on the Al-rich Beta for PNA at low temperatures, which exhibited exceptional high NO storage capacity (NPR=0.92 mol_{NO}/mol_{Pd}). Characterizations reveal that low SAR and consequently more Al pairs are responsible for more Pd^{2+} species, which resulted in high NO storage capacity. Very importantly, even after hydrothermal aging at 750 °C, 1 % Pd/Beta-4 still exhibited good NO storage capacity even higher than that of fresh conventional Beta supported Pd species. Because the Al-rich Beta was prepared in the absence of organic templates, it is believable that such Al-rich Beta would be useful in the NO_x emission-control system in HDVs in the future by combination of high performance and low cost.

CRediT authorship contribution statement

Prof. Xiangju Meng (XJM) and Prof. Feng-Shou Xiao (FSX) designed this work, Mr. Jian Li (JL) performed experiments for this work, Dr. Sen Wang (SW) and Prof. Weibin Fan (WBF) carried out DR UV–vis spectroscopic investigations for Al sites, Dr. Yulong Shan (YLS) and Prof. Hong He (HH) performed hydrothermal aging experiments. All people discussed the results, and FSX, JL, and XJM wrote the manuscript.

Declaration of Competing Interest

The authors declare that they have no known competing financial interests or personal relationships that could have appeared to influence the work reported in this paper.

Data availability

Data will be made available on request.

Acknowledgements

This work is supported by National Key Research and Development Program of China (2022YFA1503602) and National Natural Science Foundation of China (22125204, U20B6004, and 22288101).

Appendix A. Supporting information

Supplementary data associated with this article can be found in the online version at doi:10.1016/j.apcatb.2023.123127.

References

[1] C.A. Pope III, D.W. Dockery, Critical review - health effects of fine particulate air pollution: lines that connect, J. Air Waste Manag. Assoc. 56 (2006) 709–742.
[2] M.Z. Jacobson, Review of solutions to global warming, air pollution, and energy security, Energy Environ. Sci. 2 (2009) 148–173.
[3] A.Y. Wang, L. Olsson, The impact of automotive catalysis on the United Nations sustainable development goals, Nat. Catal. 2 (2019) 566–570.
[4] L. Ma, Y. Cheng, G. Cavataio, R.W. McCabe, L. Fu, J. Li, In situ DRIFTS and temperature-programmed technology study on NH-SCR of NO over Cu-SSZ-13 and Cu-SAPO-34 catalysts, Appl. Catal. B 156 (2014) 428–437.
[5] J.H. Kwak, R.G. Tonkyn, D.H. Kim, J. Szanyi, C.H. Peden, Excellent activity and selectivity of Cu-SSZ-13 in the selective catalytic reduction of NO with NH_3, J. Catal. 275 (2010) 187–190.
[6] I. Song, S. Youn, H. Lee, D.H. Kim, CeO_2-TiO_2 catalyst prepared by physical mixing for NH_3 selective catalytic reduction: evidence about the migration of sulfates from TiO_2 to CeO_2 via simple calcination, Korean J. Chem. Eng. 33 (2016) 2547–2554.
[7] L. Zhang, Q.M. Wu, X.J. Meng, F.S. Xiao, Recent advances in the preparation of 8MR zeolites for the selective catalytic reduction of NO_x (NH_3-SCR) in diesel engines, Chem. J. Chin. Univ. 41 (2018) 19–27.
[8] G. Qi, S.J. Schmieg, S. Ren, et al. Zeolite promoted silver-based catalyst for NO_x storage: U.S., 9597635. 2017–3-21.
[9] R.R. Rajaram, H.Y. Chen, D. Liu. Passive NO_x adsorber: U.S., 20150158019. 2015–6-11.
[10] B. Kearl, Q. Yin, X. Qi, et al. Zone coated catalytic substrates with passive NO_x adsorption zones: U.S., 20160045867. 2016–2-18.
[11] J.E. Collier, Y. Sanyuan. PASSIVE NO_x ADSORBER. U.S., 20170001169. 2017-1-5.
[12] T.V. Janssens, P.N. Vennestrøm. Method for producing metal exchanged zeolites by solid-state ion exchange at low temperatures. U.S., 20170095804. 2017-4-6.
[13] A.F. Chiffey, J. Corps, L. Mitchell-Downie, et al. PASSIVE NO_x ADSORBER. U.S., 20170096923. 2017-4-6.
[14] H.Y. Chen, S. Mulla. Cold Start Catalyst and Its Use in Exhaust Systems. U.S., 20170128922. 2017-5-11.
[15] M.A. Biberger, B. Kearl, Q. Yin, et al. Compositions for passive NO_x adsorption (PNA) systems and methods of making and using same: U.S., 20180093249. 2018-4-5.
[16] H.Y. Chen, D. Liu, E. Weigert, et al., Durability Assessment of Diesel Cold Start Concept (dCSC™) Technologies, SAE Int J. Eng. 10 (2017) 1713–1721.
[17] H.Y. Chen, S. Mulla, E. Weigert, K. Camm, T. Ballinger, J. Cox, P. Blakeman, Cold start concept: a novel catalyst for cold start emission control, SAE Int. J. Fuels Lubr. 6 (2013) 372–381.
[18] M. Moliner, A. Corma, From metal-supported oxides to well-defined metal site zeolites: the next generation of passive NO_x adsorbers for low-temperature control of emissions fromdiesel engines, React. Chem. Eng. 4 (2019) 223–234.
[19] Y. Ji, S. Bai, M. Crocker, Al_2O_3-based passive NO_x adsorbers for low temperature applications, Appl. Catal. B 107–171 (2015) 283–292.
[20] J.R. Theis, An assessment of Pt and Pd model catalysts for low temperature NO_x adsorption, Catal. Today 267 (2016) 93–109.
[21] S. Tamm, S. Andonova, L. Olsson, Silver as storage compound for NO_x at low temperatures, Catal. Lett. 144 (2014) 674–684.
[22] S.X. Ren, S.J. Schmieg, C.K. Koch, G.S. Qi, W. Li, Investigation of Ag-based low temperature NO adsorbers, Catal. Today 258 (2015) 378–385.
[23] J. Lee, Y. Ryou, S.J. Cho, H. Lee, C.H. Kim, D.H. Kim, Investigation of the active sites and optimum Pd/Al of Pd/ZSM-5 passive NO adsorbers for the cold-start application: evidence of isolated-Pd species obtained after a high-temperature thermal treatment, Appl. Catal. B 226 (2018) 71–82.
[24] Y.T. Gu, P.Z. Ryan, Y.R. Chen, S.E. William, Investigation of an irreversible NO_x storage degradation Mode on a Pd/BEA passive NO_x adsorber, Appl. Catal. B 258 (2019), 118032.
[25] A. Gupta, S.B. Kang, M.P. Harold, NO_x uptake and release on Pd/SSZ-13: impact of feed composition and temperature, Appl. Catal. B 258 (2019), 118032.
[26] M. Ambast, K. Karinshak, B. Md, M. Rahman, L.C. Grabow, Passive NO_x adsorption on Pd/H-ZSM-5: experiments and modeling, Appl. Catal. B 269 (2020), 118802.
[27] Y. Kim, S. Hwang, J. Lee, Y. Ryou, H. Lee, C.H. Kim, D.H. Kim, Comparison of NO_x adsorption/desorption behaviors over Pd/CeO_2 and Pd/SSZ-13 as passive NO_x adsorbers for cold start application, Emiss. Control Sci. Technol. 5 (2019) 172–182.
[28] A.Y. Wang, K.P. Xie, A. Kumar, K. Kamasamudram, L. Olsson, Layered Pd/SSZ-13 with Cu/SSZ-13 as PNA- SCR dual-layer monolith catalyst for NO_x abatement, Catal. Today 360 (2021) 356–366.
[29] P. Kunal, T.J. Toops, M.K. Kidder, M.J. Lance, Deactivation trends of Pd/SSZ-13 under the simultaneous presence of NO, CO, hydrocarbons and water for passive NO_x adsorption, Appl. Catal. B 299 (2021), 120591.
[30] K. Khivantsev, N.R. Jaegers, L. Kovarik, J.Z. Hu, F. Gao, Y. Wang, J. Szanyi, Palladium/zeolite low temperature passive NO_x adsorbers (PNA): structure-adsorption property relationships for hydrothermally aged PNA materials, Emiss. Control Sci. Technol. 6 (2020) 126–138.
[31] J. Lee, Y.S. Ryou, S.J. Cho, H.Y. Lee, C.H. Kim, D.H. Kim, Investigation of the active sites and optimum Pd/Al of Pd/ZSM-5 passive NO adsorbers for the cold-start

application: evidence of isolated-Pd species obtained after a high-temperature thermal treatment, Appl. Catal. B 226 (2018) 71–82.
[32] O. Mihai, L. Trandafilović, T. Wentworth, F.F. Torres, L. Olsson, The effect of Si/Al ratio for Pd/BEA and Pd/SSZ-13 used as passive NO_x adsorbers, Top. Catal. 61 (2018) 2007–2020.
[33] X.J. Meng, F.-S. Xiao, Green routes for synthesis of zeolites, Chem. Rev. 114 (2014) 1522–1544.
[34] B. Xie, J.W. Song, L.M. Ren, Y.Y. Ji, J.X. Li, F.-S. Xiao, Organotemplate-free and fast route for synthesizing Beta zeolite, Chem. Mater. 20 (2008) 4533–4535.
[35] B. Xie, H.Y. Zhang, C.G. Yang, S.Y. Liu, L.M. Ren, L. Zhang, X.J. Meng, B. Yilmaz, U. Muller, F.-S. Xiao, Seed-directed synthesis of zeolites with enhanced performance in the absence of organic templates, Chem. Comm. 47 (2011) 3945–3947.
[36] H.Y. Zhang, B. Xie, X.J. Meng, U. Muller, B. Yilmaz, M. Feyen, S. Maurer, H. Gies, T. Tatsumi, X.H. Bao, W.P. Zhang, D. De Vos, F.-S. Xiao, Rational synthesis of Beta zeolite with improved quality by decreasing crystallization temperature in organotemplate-free route, Microporous Mesoporous Mater. 180 (2013) 123–129.
[37] C.Y. Chen, Q.M. Wu, F. Chen, X.J. Meng, F.S. Xiao, Aluminium-rich Beta zeolite-supported platinum nanoparticles for the low-temperature catalytic removal of toluene, J. Mater. Chem. A 3 (2015) 5556.
[38] P. Sazama, B. Wichterlova, S. Sklenak, V.I. Parvulescu, N. Candu, G. Sadovska, J. Dedecek, P. Klein, V. Pashkova, P. Stastny, Acid and redox activity of template-free Al-rich H-BEA* and Fe-BEA* zeolites, J. Catal. 318 (2014) 22–33.
[39] P. Sazama, L. Mokrzycki, B. Wichterlova, A. Vondrova, R. Pilar, J. Dedecek, S. Sklenak, E. Tabor, Unprecedented propane-SCR-NO_x activity over template-free synthesized Al-rich Co-BEA / zeolite, J. Catal. 332 (2015) 201–211.
[40] X. Li, C. Shi, Z.S. Zhang, H. Gies, F.S. Xiao, D. De Vos, T. Yokoi, X.H. Bao, M. Feyen, S. Maurer, B. Yilmaz, U. Muller, W.P. Zhang, Enhancement of low-temperature activity over Cu-exchanged zeolite beta from organotemplate-free synthesis for the selective catalytic reduction of NO_x with NH_3 in exhaust gas streams, Microporous Mesoporous Mater. 200 (2014) 304–310.
[41] Y.X. Peng, L. Zhang, L. Chen, D.Z. Yuan, G.X. Wang, X.J. Meng, F.S. Xiao, Catalytic performance for toluene abatement over Al-rich Beta zeolite supported manganese oxides, Catal. Today 297 (2017) 182–187.
[42] Q.M. Wu, X. Wang, X.J. Meng, C.G. Yang, Y. Liu, Y.Y. Jin, Q. Yang, F.S. Xiao, Organotemplate-free, seed-directed, and rapid synthesis of Al-rich zeolite MTT with improved catalytic performance in isomerization of m-xylene, Microporous Mesoporous Mater. 186 (2014) 106–112.
[43] B. Yilmaz, U. Muller, M. Feyen, S. Maurer, H.Y. Zhang, X.J. Meng, F.S. Xiao, X. H. Bao, W.P. Zhang, H. Imai, T. Tokoi, T. Tatsumi, H. Gies, T.D. Baerdemaeker, D. De Vos, A new catalyst platform: zeolite Beta from template-free synthesis, Catal. Sci. Technol. 3 (2013) 2580–2586.
[44] S.V. Minnerbruggen, T.D. Baerdemaeker, K.Y. Cheung, A.N. Parvulescu, U. Muller, P. Tomkins, R.D. Oliveira-Silva, X.J. Meng, F.S. Xiao, T. Yokoi, W.P. Zhang, D. Sakellariou, D. De Vos, Alkylation of isobutane with butenes using OSDA-free zeolite beta, Catal. Today 406 (2022) 206–212.
[45] L. Xu, C. Shi, B.B. Chen, F.S. Xiao, W.P. Zhang, Improvement of catalytic activity over Cu-Fe modified Al-rich Beta catalyst for the selective catalytic reduction of NO_x with NH_3, Microporous Mesoporous Mater. 236 (2016) 211–217.
[46] L. Zhang, L. Chen, Y.B. Li, Y.X. Peng, F. Chen, L. Wang, C.B. Zhang, X.J. Meng, H. He, F.S. Xiao, Complete oxidation of formaldehyde at room temperature over an Al-rich Beta zeolite supported platinum catalyst, Appl. Catal. B 219 (2017) 200–208.
[47] H.Y. Chen, J.E. Collier, D.X. Liu, L. Mantarosie, D. Duran-Martin, V. Novak, R. R. Rajaram, D. Thompsett, Low temperature NO storage of zeolite supported Pd for low temperature diesel engine emission control, Catal. Lett. 146 (2016) 1706–1711.
[48] A. Thogersen, J. Mayandi, L. Vines, M.F. Sunding, A. Olsen, S. Diplas, M. Mitome, Y. Bando, Composition and structure of Pd nanoclusters in SiO_x thin film, J. Appl. Phys. 109 (2011), 084329.
[49] Y. Zheng, L. Kovarik, M.H. Engelhard, Y. Wang, Y. Wang, F. Gao, J. Szanyi, Low-temperature Pd/zeolite passive NO_x adsorbers: structure, performance, and adsorption chemistry, J. Phys. Chem. C 121 (2017) 15793–15803.
[50] Y. Zhu, J. Wang, Y.P. Zhai, G.R. Shen, J.Q. Wang, C. Wang, M.Q. Shen, The upgrading role of Al at T1/T2 sites in stabilizing Pd ions over Pd-beta passive NO_x adsorbers under a reducing atmosphere, Catal. Sci. Technol. 12 (2022) 3464–3473.
[51] M. Ogura, M. Hayashi, S. Kage, M. Matsukata, E. Kikuchi, Determination of active palladium species in ZSM-5 zeolite for selective reduction of nitric oxide with methane, Appl. Catal. B 23 (1999) 247–257.
[52] K. Ding, A. Gulec, A.M. Johnson, N.M. Schweitzer, G.D. Stucky, L.D. Marks, P. C. Stair, Identification of active sites in CO oxidation and water-gas shift over supported Pt catalysts, Science 350 (2015) 189–192.
[53] K.I. Hadjiivanov, G.N. Vayssilov, Characterization of oxide surfaces and zeolites by carbon monoxide as an IR probe molecule, Adv. Catal. 47 (2022) 307–511.
[54] K. Chakarova, E. Ivanova, K. Hadjiivanov, D. Klissurski, H. Knçzinger, Characterization of oxide surfaces and zeolites by carbon monoxide as an IR probe molecule, Phys. Chem. Chem. Phys. 6 (2004) 3702–3709.
[55] M. Rivallan, E. Seguin, S. Thomas, M. Lepage, N. Takagi, H. Hirata, T.-F. Starzyk, Platinum sintering on H-ZSM-5 followed by chemometrics of CO adsorption and 2D pressure-jump IR spectroscopy of adsorbed species, Angew. Chem. Int. Ed. 122 (2010) 797–801.
[56] K. Chakarova, M. Mihaylov, K. Hadjiivanov, FTIR spectroscopic study of CO adsorption on Pt-H-ZSM-5, Microporous Mesoporous Mater. 81 (2005) 305–312.
[57] K. Chakarova, M. Mihaylov, K. Hadjiivanov, Polycarbonyl species in Pt/H-ZSM-5: FTIR spectroscopic study of CO-CO co-adsorption, Catal. Commun. 6 (2005) 466–471.
[58] H.A. Aleksandrov, K.M. Neyman, K. Hadjiivanov, G.N. Vayssilov, Can the state of platinum species be unambiguously determined by the stretching frequency of an adsorbed CO probe molecule? Phys. Chem. Chem. Phys. 18 (2016) 22108–22121.
[59] Y. Zheng, L. Kovarik, M.H. Engelhard, Y. Wang, F. Gao, J. Szanyi, Low-temperature Pd/zeolite passive NO_x adsorbers: structure, performance, and adsorption chemistry, J. Phys. Chem. C. 121 (2017) 15793–15803.
[60] K. Okumura, J. Amano, N. Yasunobu, M. Niwa, X-ray absorption fine structure study of the formation of the highly dispersed PdO over ZSM-5 and the structural change of Pd induced by adsorption of NO, J. Phys. Chem. B 104 (2000) 1050–1057.
[61] A. Vu, J.Y. Luo, J.H. Li, W.S. Epling, Effects of CO on Pd/BEA passive NO_x adsorbers, Catal. Lett. 147 (2007) 745–750.
[62] A. Palazov, C. Chang, R. Kokes, The infrared spectrum of carbon monoxide on reduced and oxidized palladium, J. Catal. 36 (1975) 338–350.
[63] K. Khivantsev, F. Gao, L. Kovarik, Y. Wang, J. Szanyi, Molecular level understanding of how oxygen and carbon monoxide improve NO_x storage in palladium/SSZ-13 passive NO_x adsorbers: the role of NO^+ and Pd(II)(CO)(NO) species, J. Phys. Chem. C 122 (2018) 10820–10827.
[64] J. Pérez-Pariente, J. Sanz, V. Fornés, ^{29}Si and ^{27}Al MAS NMR study of zeolite with different Si/Al ratios, J. Catal. 124 (1990) 217–223.
[65] Q.M. Wu, X. Wang, G.D. Qi, Q. Guo, S.X. Pan, X.J. Meng, J. Xu, F. Deng, F.T. Fan, Z. C. Feng, et al., Sustainable synthesis of zeolites without addition of both organo-templates and solvents, J. Am. Chem. Soc. 136 (2014) 4019–4025.
[66] S. Mintova, V. Valtchev, T. Onfroy, C. Marichal, H. Knözinger, T. Bein, Variation of the Si/Al ratio in nanosized zeolite Beta crystals, Micropor. Mesopor. Mater 90 (2006) 237–245.
[67] A. Wang, K. Lindgren, M. Di, D. Bernin, P.A. Carlsson, M. Thuvander, L. Olsson, Insight into hydrothermal aging effect on Pd sites over Pd/LTA and Pd/SSZ-13 as PNA and CO oxidation monolith catalysts, Appl. Catal. B 278 (2020), 119315.
[68] M.A. Miguel, A. Camblor, S. Valencia, Synthesis in fluoride media and characterisation of aluminosilicate zeolite beta, J. Mater. Chem. 9 (1998) 2137–2145.
[69] K. Khivantsev, N.R. Jaegers, L. Kovarik, S. Prodinger, M.A. Derewinski, Y. Wang, F. Gao, J. Szanyi, Palladium/Beta zeolite passive NOx adsorbers (PNA): Clarification of PNA chemistry and the effects of CO and zeolite crystallite size on PNA performance, Appl. Catal. A 569 (2019) 141–148.
[70] Z. Sobalik, P. Sazama, J. Dedecek, Critical evaluation of the role of the distribution of Al atoms in the framework for the activity of metallo-zeolites in redox N_2O/NO_x reactions, Appl. Catal. A. 474 (2014) 178–185.
[71] P. Sazama, P. Klein, B. Wichterlova, S. Sklenak, L. Mokrzycki, J. Dedecek, Al-rich Beta zeolites. Distribution of Al atoms in the framework and related protonic and metal-ion species, J. Catal. 133 (2016) 102–114.
[72] L. Capek, J. Dedecek, P. Sazama, Al-rich beta zeolites. Distribution of Al atoms in the framework and related protonic and metal-ion species, J. Catal. 272 (2010) 44–54.
[73] J. Dedecek, L. Capek, D. Kaucky, Z. Sobalık, and B.Wichterlova. Siting and Distribution of the Co Ions in Beta Zeolite: A UV-Vis-NIR and FTIR Study, J. Catal. 211 (2002) 198–207.
[74] J. Kwak, D. Tran, S. Burton, J. Szanyi, J. Lee, C. Peden, Effects of hydrothermal aging on NH_3-SCR reaction over Cu/zeolites, J. Catal. 287 (2012) 203–209.
[75] C. Peden, J. Kwak, S. Burton, R. Tonkyn, D. Kim, J. Lee, H. Jen, G. Cavataio, Y. Cheng, Possible origin of improved high temperature performance of hydrothermally aged Cu/beta zeolite catalysts, Catal. Today 184 (2012) 245–251.
[76] L. Ma, C. Seo, X. Chen, K. Sun, Indium-doped Co_3O_4 nanorods for catalytic oxidation of CO and C_3H_6 towards diesel exhaust, Appl. Catal. B 222 (2018) 44–58.